

## Electronic Supplementary Information

# Electro-mechanical sensing in freestanding monolayered gold nanoparticle membranes

M. Gauvin,<sup>a</sup> J. Grisolia,<sup>a</sup> T. Alnasser,<sup>a</sup> B. Viallet,<sup>a</sup> S. Xie,<sup>b</sup> J. Brugger<sup>b</sup> and L. Ressier<sup>\*a</sup>

<sup>a</sup>*Université de Toulouse, LPCNO, INSA-CNRS-UPS, 135 avenue de Rangueil, Toulouse 31077, France.*

<sup>b</sup>*Microsystems Laboratory, École Polytechnique Fédérale de Lausanne, Station 17, 1015 Lausanne, Switzerland.*

\*Corresponding author: [laurence.ressier@insa-toulouse.fr](mailto:laurence.ressier@insa-toulouse.fr)

## Structural characterization of freestanding monolayered membranes of 7 nm dodecanethiol coated gold nanoparticles

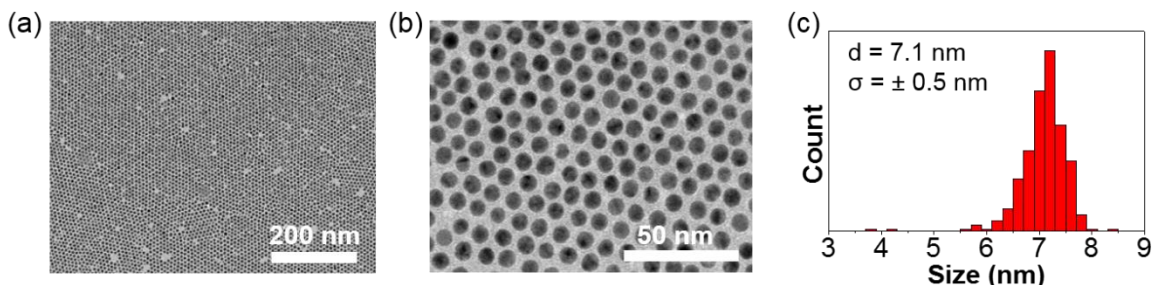


**Fig S1:** (a) Wide and (b) close-up views by transmission electron microscopy (TEM) of a freestanding monolayered membrane of 7 nm dodecanethiol coated gold nanoparticles (NPs) organized with a hexagonal close-packed structure, (c) TEM size distribution of the dodecanethiol coated gold NPs.

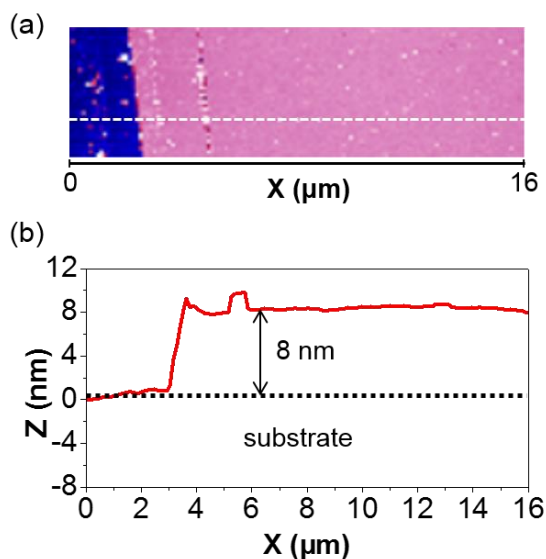


**Fig S2:** (a) Atomic force microscopy (AFM) topography image in PeakForce tapping and (b) corresponding profile (along the white dashed line on (a)) of a scratched 7 nm gold NP membrane deposited on a plain SiO<sub>2</sub> substrate.

**Mechanical characterization of a 5  $\mu\text{m}$  wide freestanding monolayered membrane of 7 nm dodecanethiol coated gold nanoparticles**

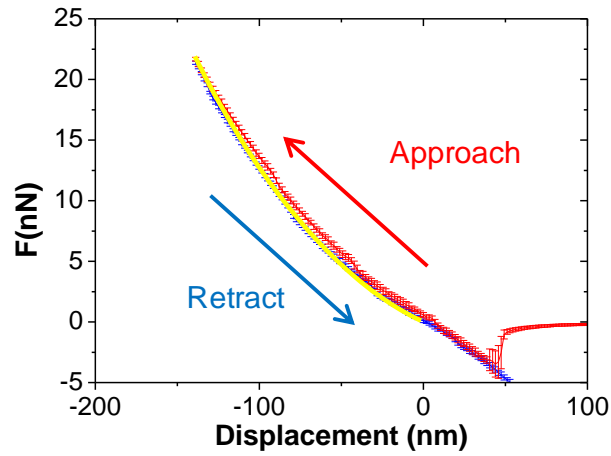


**Fig S3:** Elastic force-displacement curve on a 5  $\mu\text{m}$  wide freestanding gold NP monolayered membrane, performed by AFM force spectroscopy. This curve was obtained by averaging ten measurements carried out in the center of the same membrane. The continuous yellow line shows the fitting force-displacement curve obtained from finite element modeling with optimized membrane mechanical parameters:  $E=1.2 \pm 0.4$  GPa and  $\sigma_0=7 \pm 1$  MPa.

## Discussion on the charging energy model for Arrhenius type temperature dependence

Our results show that the electronic transport within the NP membranes is of Arrhenius type ( $\gamma=1$ ). In this regime, the electrical resistance of NP arrays is often described by a simple thermally activated behavior that gives the subsequent zero-voltage resistance:

$$R \propto \exp\left[\left(\frac{E_a}{kT}\right)\right] \quad (1)$$

where  $E_a$ , the activation energy, is often considered in the literature to represent a good estimation of the Coulomb charging energy  $E_C$  that is related to the system capacitance  $C$  by the relation  $E_C=e^2/2C$ . It is then possible to relate the experimental  $R(T)$  measurements with the properties of the nanoparticle assembly and to their environment. For a nanoparticle in an array of nanoparticles, this capacitance  $C$  is strongly influenced by the particle radius  $r$ , the interparticle distance  $l$ , the dielectric constant of the surroundings  $\epsilon_r$ , and by the number of nearest-neighbors  $N$ . However, in the literature, studies which have examined the effect of the interparticle distance on the  $E_C$  value, and therefore  $C$ , remain controversial since some report a small influence of the length of the ligand<sup>1</sup> while others infer a very strong influence.<sup>2</sup> These differences can arise from the models which are used to calculate the NP charging energy in assemblies.

Most experiments consider the capacitance of an isolated sphere:<sup>3-5</sup>

$$C = 4\pi\epsilon_0\epsilon_r r \quad (2)$$

where  $r$  is the radius of the NP,  $\epsilon_0$  is the vacuum permittivity, and  $\epsilon_r$  is the relative dielectric constant of the matrix.

Refined models were then proposed by Abeles *et al.* by taking the interparticle distance  $l$  into account:<sup>6</sup>

$$C = 4\pi\epsilon_0\epsilon_r r \left(\frac{r+l}{l}\right) \quad (3)$$

and by Beecher *et al.*<sup>7,8</sup>

$$C = 2N\pi\epsilon_0\epsilon_r r \cdot \ln\left(1 + \frac{2r}{l}\right) \quad (4)$$

where  $N$  is the number of NPs surrounding a given particle (e.g.  $N = 12$  and  $6$  for a 3D and 2D dense fcc packing respectively) and  $l$  is the interparticle distance.

Leroy and Cordan proposed a different model based on the charge image method.<sup>9,10</sup> This approach describes the capacitance between two junctions by a capacitance matrix taking into account the influence capacitance formed by two nanospheres. Such a system of two conductors is then characterized from an electrostatically point of view by the following capacitance matrix:

$$\begin{pmatrix} C_{1,1} & -C_{1,2} \\ -C_{2,1} & C_{2,2} \end{pmatrix} \quad (5)$$

where  $C_{2,1}=C_{1,2}$  and  $C_{i,i}$  represents the capacity of an isolated sphere.

For nanospheres with equal diameter  $d$  and separated by the  $l$  distance, the junction capacitance  $C_p$  between two NPs is given by the equation:

$$C_p = 4\pi\epsilon_0\epsilon_r r \sinh\left(\operatorname{acosh}\left(1 + \frac{l}{d}\right)\right) \times \sum_{n=1}^{\infty} \left[\sinh\left(2n \operatorname{acosh}\left(1 + \frac{l}{d}\right)\right)\right]^{-1} \quad (6)$$

The total system capacitance  $C$  can then be obtained by the  $C = NC_p$  where  $N$  is the number of surrounding nanoparticles. In equations (2-6), many parameters such as  $d$ ,  $l$ ,  $\epsilon_r$  ... allow adjusting the experimental values to these different models, that is probably why the literature is so controversial. It is then necessary to understand where these models come from and what their limits are.

The model of the isolated sphere only takes into account the self-capacitance of the nanoparticles and ignores the capacitance between neighboring nanoparticles, leading to an overestimated value of the Coulomb charging energy. This model cannot clearly represent our dense nanoparticle assemblies.

The Abeles model assumes a metal nanoparticle surrounded by a layer of a dielectric material with the thickness  $l$  and another infinite concentric metal layer, which overestimates the contribution of the mutual capacitance between neighboring nanoparticles and thus an underestimated Coulomb charging energy.

Beecher's model is based on experiments derived from a nanosphere and a STM tip whose diameter can be considered as infinite with respect to the nanoparticle radius.<sup>7,11</sup> Beecher's expression hence represents the interaction capacity between an infinite plane and a nanosphere, which is not realistic to describe our nanoparticle assemblies. More importantly, this model lacks of self-consistency because the capacitance tends to 0 if the interparticle distance grows and tends to infinity, which is not realistic since it would tend to the capacity value of the isolated sphere.

Thus, the only self-consistent model is the Leroy-Cordan's model which is the only one to take into account the mutual interactions between spheres and respect the self-capacity condition:

$$\lim_{l \rightarrow \infty} C_{i,i} = 4\pi\epsilon_0\epsilon_r r \quad (7)$$

where the distance  $l$  between the nanospheres becomes very large. In our case, the Leroy-Cordan's model leads to an  $E_c$  value of 25 meV which is in very good agreement with values determined experimentally when considering an average Au NP diameter  $d = 2r = 7.1$  nm, an interparticle distance  $l = 1.3$  nm as deduced from SEM images (Fig. 2c and 2d),  $\epsilon_r = 2.3$  typical for alkanethiol self-assembled monolayers ( $\epsilon_r = 2.7 \pm 0.3$ )<sup>12</sup> and  $N = 6$  for a monolayered hexagonal array.

## Numerical simulation of the strain-induced resistance variations in freestanding nanoparticle membranes

The electronic conduction within the freestanding monolayered NP membranes was modelled using a home-made routine on Scilab. A  $5\ \mu\text{m} \times 5\ \mu\text{m}$  hexagonally-packed 2D array of 7.1 nm NPs separated by an interparticle distance  $l=1.3\ \text{nm}$  at zero strain, was contacted between two electrodes: one connected to the center of the array and polarized at 1 V and one connected to the ground at the edge of the NP array. Each NP  $i$  in the array was defined by a given position  $(x_i, y_i, z_i)$  and considered as a node of a network of resistors  $R_{ij}$  (Fig. S4).

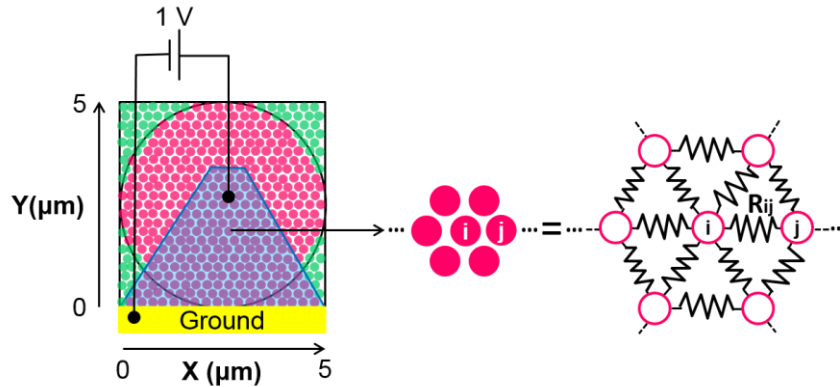


**Fig. S4:** From left to right: Schematic of a  $5\ \mu\text{m} \times 5\ \mu\text{m}$  monolayered hexagonal array of 7.1 nm Au NPs separated by an interparticle distance of 1.3 nm at rest. Inside the circular membrane area, NPs depicted as pink circles underwent deformation while outside the membrane, NPs depicted by green circles were fixed. The NP array was contacted in the center and at the lower edge of the membrane by two electrodes to mimic the conductive AFM experiments. An equivalent network of resistors was built upon the monolayered hexagonal NP array located inside the blue-colored area and used for the simulation of the electrical current under 1 V polarization and the strain-induced resistance variations.

The electrical resistance  $R_{ij}$  between the nodes  $i$  and  $j$  was computed following the simple equation  $R_{ij} \propto e^{\beta l_{ij}}$ , where  $\beta$  is the tunnel decay constant and  $l_{ij}$  is the edge-to-edge interparticle distance between the NPs  $i$  and  $j$ . This simplified equation is valid since we were only concerned with the relative variations of the resistance and the contribution from the strain-induced variations of the charging energy  $Ec$  is negligible. The local displacement field of the membranes under point-loading as determined by FEA simulations (see Inset of Fig. 3b of the manuscript) was used to obtain the change in the interparticle length  $l_{ij}$  between NPs. To increase the computation speed, calculations were performed in a delimited area of the resistor network indicated as the blue-colored area in Fig. S4, enclosed between the center of the NP membrane and the ground electrode. The  $\beta$  value was fixed at  $5\ \text{nm}^{-1}$  to match the total simulated strain-induced resistance variation with that of the freestanding NP membranes experimentally measured by AFM-based experiments. The voltage at each node of the NP assembly was computed by resolving the equation  $[I] = [G][V]$  where  $V$  was the vector representing the voltage at each node,  $I$  the injected current

vector with  $I_{i=0} = 1$  and  $I_{i \neq 0} = 0$  and  $G$  the conductance matrix. The non-diagonal term  $G_{ij}$  of the matrix  $G$  was the opposite of the conductance between nodes  $i$  and  $j$ , and the diagonal term  $G_{ii}$  is the sum of all conductance values of the resistors connected to node  $i$ . The macroscopic resistance  $R$  of the whole NP assembly was then computed. The result is a value of the relative resistance of the NP membrane contacted by two external electrodes. The corresponding electrical current and local strain are shown in Fig. S5 for a point-load actuation of 21 nN in the center of the NP membrane. They are both maximum in the center of the membrane and drop toward the ground electrode.

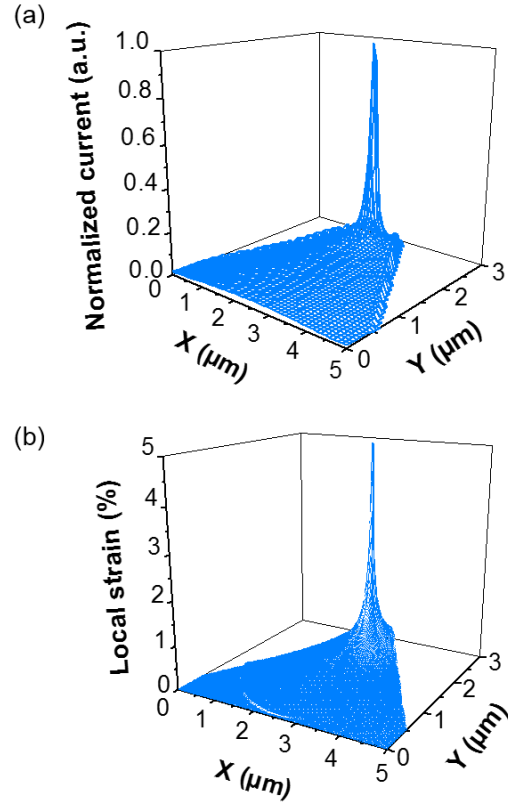


**Fig. S5:** Mappings of the simulated (a) normalized electrical current and (b) local strain in a 5 μm wide hexagonally packed NP membrane polarized at 1 V and under a point-load actuation of 21 nN.

## REFERENCES

- 1 Moreira, H.; Yu, Q.; Nadal, B.; Bresson, B.; Rosticher, M.; Lequeux, N.; Zimmers, A.; Aubin, H. Electron Cotunneling Transport in Gold Nanocrystal Arrays. *Phys. Rev. Lett.* **2011**, 107.
- 2 Dugay, J.; Tan, R. P.; Ibrahim, M.; Garcia, C.; Carrey, J.; Lacroix, L.-M.; Fazzini, P.-F.; Viau, G.; Respaud, M. Charge Transport and Interdot Coupling Tuned by the Tunnel Barrier Length in Assemblies of Nanoparticles Surrounded by Organic Ligands. *Phys. Rev. B* **2014**, 89.
- 3 Tran, T.; Beloborodov, I.; Hu, J.; Lin, X.; Rosenbaum, T.; Jaeger, H. Sequential Tunneling and Inelastic Cotunneling in Nanoparticle Arrays. *Phys. Rev. B* **2008**, 78.
- 4 Noda, Y.; Noro, S.; Akutagawa, T.; Nakamura, T. Electron Transport in a Gold Nanoparticle Assembly Structure Stabilized by a Physisorbed Porphyrin Derivative. *Phys. Rev. B* **2010**, 82.
- 5 Kang, M. S.; Sahu, A.; Norris, D. J.; Frisbie, C. D. Size- and Temperature-Dependent Charge Transport in PbSe Nanocrystal Thin Films. *Nano Lett.* **2011**, 11, 3887–3892.
- 6 Abeles, B.; Sheng, P.; Coutts, M. D.; Arie, Y. Structural and Electrical Properties of Granular Metal Films. *Adv. Phys.* **1975**, 24, 407–461.
- 7 Beecher, P.; Quinn, A. J.; Shevchenko, E. V.; Weller, H.; Redmond, G. Insulator-to-Metal Transition in Nanocrystal Assemblies Driven by in Situ Mild Thermal Annealing. *Nano Lett.* **2004**, 4, 1289–1293.
- 8 Black, C. T. Spin-Dependent Tunneling in Self-Assembled Cobalt-Nanocrystal Superlattices. *Science* **2000**, 290, 1131–1134.
- 9 Leroy, Y. Transport Électronique Dans Les Nanostructures Fortement Désordonnées, Université Louis Pasteur - Strasbourg 1, 2001.
- 10 Cordan, A. S. Occurrence of Giant Current Fluctuations in 2D Tunnel Junction Arrays. *Solid-State Electron.* **2004**, 48, 445–452.
- 11 Laikhtman, B.; Wolf, E. L. Tunneling Time and Effective Capacitance for Single Electron Tunneling. *Phys. Lett. A* **1989**, 139, 257–260.
- 12 Rampi, M. A.; Schueller, O. J. A.; Whitesides, G. M. Alkanethiol Self-Assembled Monolayers as the Dielectric of Capacitors with Nanoscale Thickness. *Appl. Phys. Lett.* **1998**, 72, 1781.